Asociación Argentina
de Mecánica Computacional

Mecánica Computacional Vol XXVII, págs. 3151-3167 (artículo completo)
Alberto Cardona, Mario Storti, Carlos Zuppa. (Eds.)
San Luis, Argentina, 10-13 Noviembre 2008

SPATIAL – TIME ADAPTIVE PROCEDURE FOR TRANSONIC FLOWS OVER A CLIPPED DELTA WING

Gustavo Bono[a], Armando M. Awruch[b] and Tales L. Popiolek[c]

[a]*Federal University of Rio Grande do Sul, Graduate Program in Mechanical Engineering, Av. Sarmento Leite 425, 90050-170 Porto Alegre, RS, Brazil, bonogustavo@gmail.com, http://www.mecanica.ufrgs.br/promec*

[b]*Federal University of Rio Grande do Sul, Applied and Computacional Mechanical Center, Av. Osvaldo Aranha 99, 90035-190 Porto Alegre, RS, Brazil, amawruch@ufrgs.br, http://www.ppgec.ufrgs.br/cemacom*

[c]*Federal Universitary Foundation of Rio Grande, Mathematical Departament, Av. Itália km 8, Campus Carreiros, 96201-900 Rio Grande, Brazil, dmttales@furg.br, http://www.furg.br*

Keywords: Transonic flow, finite element method, adaptive mesh strategy, multi-time step integration technique.

Abstract. An algorithm which combines an automatic adaptive mesh strategy and explicit multi-time steps integration technique on three-dimensional unstructured meshes is presented. These techniques are applied employing Euler equations. The flow is simulated using the Finite Element Method with an explicit one-step Taylor-Galerkin scheme and linear tetrahedral elements. The numerical solution behaviour is analyzed using error indicators to map regions where some physical phenomena, having high gradients, take place and then the adaptive process is applied to these regions. The capability and efficiency of the time-spatial adaptive procedures are compared with experimental data and with those obtained when a unique global time step is used.

1 INTRODUCTION

Over the past forty years, there has been an intense research activity in the area of computational fluid dynamics (CFD). A large proportion of this activity has been driven by the aerospace industry, with its requirements for highly accurate solutions at minimum computational cost. Recent developments in numerical methods and their applications permit to solve complex and realistic geometries and configurations for compressible flows. The demand to solve finely detailed models has challenged many researchers to come up with new and efficient tools. The spatial and time adaptive methods have been demonstrated as useful means to obtain efficient solutions of the Euler and Navier-Stokes equations.

An adaptive mesh strategy has the potential to give numerically accurate and computationally efficient solutions, because the mesh is only locally refined at places where it is necessary. The methods of mesh adaptation can be separated into three general categories: *r*, *h* and *p*. In adaptive meshes using the *r* technique, the numbers of nodes in the computational domains remains fixed and are simply redistributed, so that regions with some specified characteristics are better resolved. In *h*-refinement or mesh enrichment, nodes are added to regions of relatively large solution error by dividing locally the elements which make up the mesh or by embedding finer meshes in these regions. In adaptive meshes using the *p* adaption method, the degree of the basis function is locally adjusted to match the variation in problem solution. Although the above methods were initially designed to be applied in a separate manner, the combination of such strategies may lead to very effective schemes. Most of these subjects are well summarized in Löhner (2001), where many references are given. In this work an *h*-refinement technique is adopted.

Time integration, for instance, can be performed in one of the two classical approaches, explicit or implicit techniques. Implicit methods are computationally more expensive in terms of computer memory, but they have less stringent stability bounds with respect to explicit schemes. Explicit methods are relatively simple to code and implement, and they are easily cast in a form suitable for efficient parallelization but they are limited to a very small time step, which is based on the smallest element size in the mesh, due to the Courant-Friedricks-Lewy (CFL) stability condition. If the time step is consequently significantly reduced, run times are greatly increased due only to this small element in the entire domain. In many cases it is necessary to use a very small global time step due to the need to accurately capture phenomena exhibiting high gradients of one or more variables.

To improve the performance of explicit schemes a time adaptive technique with sub-cycles may be used. Standard explicit schemes use a globally minimum time step for stability reason. This implies that many of the elements, such as elements having large volumes, are being advanced at a fraction of the maximum time step permitted locally by stability considerations.

Several mixed time integration methods have been implemented and they are based in previous work in the field of structural dynamics (see Hughes and Liu, 1978; Belytschko et al., 1979; Belytschko and Gilbertsen, 1992; Belytschko and Lu, 1993). These methods are efficient because they are used in the entire mesh but with different time steps in different parts of the mesh, adapted to the local physics or local numerical restrictions.

Within the field of CFD and in the context of the Finite Element Method (FEM) an early work was developed by Löhner et al. (1984). In this work, the reduction in processing time was about 2 and 4 times for an inviscid two-dimensional problem with an explicit-explicit methods (sometimes referred as a multi-time stepping technique using sub-cycles). Chang et al. (1993) proposed an implicit-explicit method for viscous and inviscid two-dimensional problems; the time adaptive algorithm was between 1.1 and 7.1 times faster than the algorithm

which uses an unique global time step. In the implicit-explicit methods, the implicit and explicit integration methods are combined in the different parts of the mesh to obtain an optimal time-integration scheme. Maurits et al. (1998) studied the stability and accuracy for the one-dimensional convection-diffusion equation using the multi-time stepping method.

Based on the time adaptive method proposed by Belytschko and Gilbertsen (1992), Teixeira and Awruch (2001) implemented this technique for inviscid compressible problem for tetrahedral elements. The algorithm has the possibility to control the time step using the same criteria (or indicators of flow characteristics) employed by Argyris et al. (1990). The time step in the elements is reduced when the indicators identify possibilities of numerical instability or a significative loss of accuracy of the solution.

In the context of the Finite Volume Method, some major contribution were developed by Hokker et al. (1992), van der Ven et al. (1997) and Wackers and Koren (2003), among others

In this paper, the application of the unstructured mesh refinement with the multi-time steps technique to analyze the flow about an inviscid transonic clipped delta wing is presented. Two cases are shown to illustrate the capability of the sub-cycling technique and results are compared with experimental results available in the literature. Although the work presented here is based on an inviscid flow with tetrahedral elements, the time adaptive method was also developed for viscous flows and hexahedral elements.

2 THE GOVERNING EQUATIONS

Let $\Omega \subset R^{n_{sd}}$ and (0,T) be the spatial and temporal domains, respectively, where $n_{sd} = 3$ is the number of space dimensions, and let Γ denote the boundary of Ω. The spatial and temporal coordinates are denoted by **x** and t. We consider the Euler equations governing unsteady compressible flows with no source terms, written here in their dimensionless form as

$$\frac{\partial \mathbf{U}}{\partial t} + \frac{\partial \mathbf{F}_i}{\partial x_i} = 0 \tag{1}$$

where **U,** is the unknown vector of the conservation variables, and $\mathbf{F}_i$, the convective flux vector, are defined as

$$\mathbf{U} = \begin{Bmatrix} \rho \\ \rho v_i \\ \rho e \end{Bmatrix}, \qquad \mathbf{F}_i = \begin{Bmatrix} \rho v_j \\ \rho v_i v_j + p\,\delta_{ij} \\ v_j\left(\rho e + p\right) \end{Bmatrix} \tag{2}$$

with *i, j = 1,2,3*. Here v_i is the velocity component in the direction of the coordinate x_i, ρ is the specific mass, p is the thermodynamic pressure, e is the total specific energy and δ_{ij} is the Kronecker delta function. For a compressible fluid flow, the following non-dimensional scales are used

$$\begin{aligned} x_i &= \frac{\tilde{x}_i}{\tilde{L}_\infty} \qquad v_i = \frac{\tilde{v}_i}{\tilde{a}_\infty} \qquad \rho = \frac{\tilde{\rho}}{\tilde{\rho}_\infty} \qquad e_i = \frac{\tilde{e}_i}{\tilde{a}_\infty^2} \\ p &= \frac{\tilde{p}}{\tilde{\rho}_\infty\,\tilde{a}_\infty^2} \qquad i = \frac{\tilde{c}_v\,\tilde{T}}{\tilde{a}_\infty^2} \qquad t = \frac{\tilde{t}}{\tilde{L}_\infty / \tilde{a}_\infty} \end{aligned} \tag{3}$$

where a superscript $\sim$, indicates a dimensional quantity, a subscript ∞ represents a reference free stream value, a is a speed of sound and L is a reference length.

Assuming that air behaves as a calorically perfect gas, the pressure, which is calculated by the equation of state, and internal energy *i* are given by the following equations

$$p = (\gamma - 1)\rho\, i\,, \qquad i = c_v T = e - \frac{1}{2} v_i\, v_i \tag{4}$$

where T is the temperature and the specific heat ratio $\gamma = c_p / c_v$ is assumed to be constant and equal to 1.4. The corresponding quasi-linear form of equations (1) is

$$\frac{\partial \mathbf{U}}{\partial t} + \mathbf{A}_i \frac{\partial \mathbf{U}}{\partial x_i} = 0\,, \qquad \text{with} \qquad \mathbf{A}_i = \frac{\partial \mathbf{F}_i}{\partial \mathbf{U}} \tag{5}$$

where $\mathbf{A}_i$ is the convection Jacobian defined as $\mathbf{A}_i = \partial \mathbf{F}_i / \partial \mathbf{U}$ (Hughes and Tezduyar, 1984). Initial and boundary conditions must be added to equation (5) in order to define uniquely the problem.

3 A TAYLOR-GALERKIN FORMULATION

The numerical scheme is obtained expanding in Taylor series the governing equation and applying after the space discretization process, using the Finite Element Method (FEM) in the context of the classical Bubnov-Galerkin scheme. This approach could be interpreted as the finite element version of the Lax-Wendroff scheme, used in finite differences. An explicit one-step scheme is employed for solving the compressible inviscid flow problems. In the finite element method the flow field is subdivided into a set of non-overlapping elements which cover the whole domain without gaps.

This time integration provides second-order accuracy in time. The formulation exclusively employs tetrahedral finite elements which provide second-order spatial accuracy. Linear unstructured finite elements were chosen because they can be easily generated for complex geometries and exactly integrated without numerical quadrature.

The one-step Taylor-Galerkin scheme presented here is similar to that presented by Donea (1984). Expanding the conservation variables $\mathbf{U}$ at $t = t^{n+1}$ in Taylor series including the first and second derivatives, the following expression is obtained

$$\Delta \mathbf{U}^{n+1} = \Delta t \left(\frac{\partial \mathbf{U}}{\partial t}^{n} + \frac{1}{2} \frac{\partial\, \Delta \mathbf{U}}{\partial t}^{n+1} \right) + \frac{\Delta t^2}{2} \left(\frac{\partial^2 \mathbf{U}}{\partial t^2}^{n} + \frac{1}{2} \frac{\partial^2\, \Delta \mathbf{U}}{\partial t^2}^{n+1} \right) \tag{6}$$

with $\Delta \mathbf{U}^{n+1} = \mathbf{U}^{n+1} - \mathbf{U}^{n}$, n and $n+1$ indicates t and $t+\Delta t$, respectively. More details can be found in Bono (2008). Substituting equation (1) and its second derivative into equation (6), and neglecting high-order terms, it is obtained

$$\begin{aligned} \Delta \mathbf{U}_{I+1}^{n+1} = \Delta t \left[-\frac{\partial \mathbf{F}_i}{\partial x_i}^{n} + \frac{\Delta t}{2} \frac{\partial}{\partial x_k} \left(\mathbf{A}_k{}^{n} \frac{\partial \mathbf{F}_i}{\partial x_i}^{n} \right) \right] + \\ + \frac{\Delta t}{2} \left[-\frac{\partial\, \Delta \mathbf{F}_{iI}}{\partial x_i}^{n+1} + \frac{\Delta t}{2} \frac{\partial}{\partial x_k} \left(\mathbf{A}_k{}^{n} \frac{\partial\, \Delta \mathbf{F}_{iI}}{\partial x_i}^{n+1} \right) \right] \end{aligned} \tag{7}$$

where I is an iteration counter, $\Delta \mathbf{F}_i^{n+1} = \mathbf{F}_i^{n+1} - \mathbf{F}_i^{n}$ and $\mathbf{A}_i$ is the convection Jacobian defined as $\mathbf{A}_i = \partial \mathbf{F}_i / \partial \mathbf{U}$ (Hughes and Tezduyar, 1984). In expression (7), the variables at time level $n+1$ are involved in the left and right sides of the equation; therefore, it is necessary to use an

iterative scheme.

Applying the classical Bubnov-Galerkin weighted residual method in the context of the FEM to equation (7), the spatial discretization is obtained. The computational domain was divided into a finite number of linear tetrahedral elements (unstructured mesh). The consistent mass matrix, **M**, is substituted by the lumped mass matrix, $\mathbf{M}_L$, and then these equations are solved with an explicit scheme. The explicit matrix form of equations (7) becomes (Bono, 2008)

$$\mathbf{M}_L\ \Delta\bar{\mathbf{U}}_{I+1}^{n+1} = \Delta t\left[-\mathbf{B}_i\,\bar{\mathbf{F}}_i - \frac{\Delta t}{2}\mathbf{C}_i\,\bar{\mathbf{F}}_i + \frac{\Delta t}{2}\boldsymbol{g}\right]^n + \frac{\Delta t}{2}\left[-\mathbf{B}_i\,\Delta\bar{\mathbf{F}}_{iI} - \frac{\Delta t}{2}\mathbf{C}_i\,\Delta\bar{\mathbf{F}}_{iI}\right]^{n+1} \tag{8}$$

where the element matrices can be written as follows

$$\begin{aligned}
\mathbf{M} &= \int_{\Omega_e} \mathbf{N}^T\,\mathbf{N}\,d\Omega \\
\mathbf{B}_i &= \int_{\Omega_e} \mathbf{N}^T\,\mathbf{N}_{,i}\,d\Omega \\
\mathbf{C}_i &= \int_{\Omega_e} \mathbf{N}_{,k}^T\ \mathbf{A}_k{}^n\,\mathbf{N}_{,i}\,d\Omega \\
\mathbf{g}^n &= \int_{\Gamma_e} \hat{\mathbf{N}}^T\mathbf{A}_k^n\,n_k\left(\mathbf{N}_{,i}\,\bar{\mathbf{F}}_i^n\right)d\Gamma
\end{aligned} \tag{9}$$

with **N** being the shape functions, $\mathbf{N}_{,i} = \partial\mathbf{N}/\partial x_i$ and n_k is the cosine of the angle formed by the outward normal axis to the boundary Γ_e.

The proposed schemes are conditionally stable, and the local stability condition for element *E* is given by

$$\Delta t_E = CS\,\frac{L_E}{a + \left(v_i\,v_i\right)^{1/2}} \tag{10}$$

where L_E is a characteristic dimension of the element, *a* is the sound speed and *CS* is a safety coefficient (in this work, CS = 0.1 is adopted).

At transonic and supersonic speeds, an additional numerical damping is necessary to capture shocks and to smooth local oscillations in the vicinity of shocks. An artificial viscosity model, as proposed by Argyris et al. (1990), due to its simplicity and efficiency in terms of CPU time, is adopted here. An artificial viscosity is added explicitly to the non-smoothed solution as follows

$$\mathbf{U}_s^{n+1} = \mathbf{U}^{n+1} + \mathbf{M}_L{}^{-1}\mathrm{D} \tag{11}$$

where $\mathbf{M}_L$ is the assembled lumped mass matrix, $\mathbf{U}_s^{n+1}$ and $\mathbf{U}^{n+1}$ are the smoothed and non-smoothed solutions at $t + \Delta t$, respectively. The vector D is given by

$$\mathrm{D} = \sum_{\mathrm{ele}} \mathrm{CFL}\ \mathrm{CAF}\ S_{ele}\left[\mathbf{M} - \mathbf{M}_L\right]_{ele}\ \mathbf{U}_{ele}^n \tag{12}$$

where *ele* is an index referred to a specific element, $\mathrm{CFL} = \Delta t/\Delta t_E$ is the local Courant-Friedrichs-Lewy number, CAF is an artificial damping coefficient given by the user, S_{ele} is a pressure sensor at element level obtained as an average of nodal values S_i. Values of S_i are

components of the following assembled global vector

$$S_{\mathrm{i}} = \sum_{\mathrm{ele}} \frac{\left|\left(\mathbf{M}-\mathbf{M}_L\right)_{ele}\mathbf{p}\right|_i}{\left[\left|\mathbf{M}-\mathbf{M}_L\right|_{ele}\mathbf{p}\right]_i} \tag{13}$$

where $\mathbf{p}$ is the pressure vector of a specific element, the symbol $|\cdot|$ indicates that absolute values of the corresponding terms must be taken and, finally, $\mathbf{M}$ is the consistent mass matrix at element level.

The constant CAF must be specified with care in order to avoid interferences of artificial and physical viscosities. In this work $\mathrm{CAF} = 1.0$ is adopted.

4 SPATIAL ADAPTIVE METHOD

The unstructured mesh adaptation has the potential to give numerically accurate and computationally efficient solutions, because the mesh is only locally refined at the places of interest. An adaptive mesh strategy basically is characterized by error indicators, an adaptive criterion and a refinement scheme.

Errors indicators are used to identify the characteristics and behaviour of the numerical solutions in order to determine regions of the computational domain where a refinement process is necessary, looking for an accurate solution. In this work, these error indicators take into account regions with velocity gradients, pressure gradients and specific mass gradients. The criterion for mesh adaptation is based in the normal distribution of the error indicators and their mean values and standard deviation. The adaptive process was performed using the *h*-refinement method. Elements refined are divided in eight new elements; this type of refinement is defined as a regular refinement, and it is represented by 1:8. To close the refinement scheme and to avoid hanging nodes, it is necessary to perform irregular refinements in neighbour elements, represented by 1:2, 1:3 or 1:4. Elements having less than four edges divided by new nodes, created as a consequence of the adaptation scheme applied to their neighbour elements, are submitted to irregular refinements. However, if an element has four or more edges divided by new nodes, it is submitted to a regular refinement. In order to improve the geometric quality of the elements in the finite element mesh and to smooth the transition among elements of different size a smoothing technique with node re-allocations could be included. Details of the error indicators, mesh adaptation and the refinement process can be found in Popiolek and Awruch (2006).

This adaptive scheme has been validated with respect to analytical and experimental results for several regimes of incompressible and compressible flows (Popiolek and Awruch, 2006; Bono, Popiolek and Awruch, 2007; Bono, 2008).

5 THE MULTI-TIME STEPS TECHNIQUE USING SUB-CYCLES

A time adaptive technique is employed with unstructured mesh flow solvers, in a similar form to the spatial adaptive unstructured mesh refinement, to solve more efficiently the physics of the flow in time. The time adaptive method (which could be called also multi-time steps with sub-cycles) is implemented considering the critical time step for each element in the domain. To facilitate the integration, elements are divided into groups according to their time step. Element groups can be integrated with different time steps, and they are subject to the following restrictions:

- all group of time steps must be integer multiples of each other, allowing elements to be stored in groups according to their critical time steps and no by their physical

proximity;
- if any node is connected to elements of different groups, the time step of these element groups must be integer multiples of the time step belonging to the group having the smallest time interval.

To initiate the time adaptive method, time step node groups (Δt_N) and time step element groups (Δt_G) are determined at the beginning of the solution. The control time step (master time increment) is taking as being equal to the largest time step in the elements groups and is used to determine when a cycle has been completed. In the control time step all variables are in the same time of the physical problem, therefore the time adaptive procedure implemented here should be employed for unsteady problems.

The sub-cycle method can be summarized in the following steps:

1 – The procedure is initiated by determining the critical time step for each element i (Δt_{Ei}) with equation (10) and the corresponding minimum value Δt_{Emin} is found. To each element is then assigned an integer multiple value n_{Ei}, which corresponds to the relation

$$n_{Ei} = \text{int}\left(\frac{\Delta t_{Ei}}{\Delta t_{E\min}}\right) \quad \text{with } i = 1,...,nele \tag{14}$$

where *nele* is the total number of elements.

2 – After the local time steps have been determined for each element, the elements are collected into groups based on their local time step. After the time step Δt_N for each node N are computed, considering the smallest time step corresponding to all elements e connected to node N, the node time step is determined by

$$\Delta t_N = \min_e \left(n_{Ee}\, \Delta t_{E\min}\right) \tag{15}$$

In this work, the procedure is similar to that proposed by Löhner et al. (1985) and also employed by Teixeira and Awruch (2001). Elements in each group g march in time at a constant time step equal to $\Delta t = 2^{(g-1)}\, \Delta t_{E\min}$. The procedure is performed by placing all elements i, with $\Delta t_{E\min} \le \Delta t_i < 2\Delta t_{E\min}$ into group 1 and assigning to these elements the time step Δt_{Emin}, all elements with $2\Delta t_{E\min} \le \Delta t_i < 4\Delta t_{E\min}$ into group 2 and assigning to these elements the time step $2\Delta t_{Emin}$, and so on.

3 – Finally, the time step for each element Δt_G are re-evaluated considering that a specific element has the smallest time step of all the time steps corresponding to nodes belonging to this element.

The time adaptive method implemented here has three clocks: the first clock is assigned to the current time (*time*), the second is assigned to the node group (t_N) and the third clock is assigned to the element group (t_G). These clocks, when compared to the current time, indicate when a node or group of elements is ready to be updated. At the beginning of each sub-cycle, the nodal and element group clocks are advanced for those nodes and element groups which were updated in the previous sub-cycle. All nodes and element groups are updated in the first sub-cycle.

Once the nodal and element group clocks have been updated, the integration procedure continues. Each element group whose clock is behind the current time $t_G \le time$ will be updated. After all elements groups have been updated, the nodal loop is executed. Each node group whose clock is behind the current time $t_N \le time$ will be updated.

This updating procedure can be visualized easily with a simplified example. Consider a mesh which has five one-dimensional elements in three groups (g = 1, 2 and 3) with the following initial time step $1\Delta t$, $2\Delta t$, $2\Delta t$, $4\Delta t$ and $4\Delta t$. Applying stages 1, 2 and 3, previously described, the following node and element groups are obtained (see Figure 1a): Δt_N = {1, 1, 2, 2, 4, 4} and Δt_G = {1, 1, 2, 2, 4}, respectively. It should be noted that the time step of the cycle is $t_c = 4\Delta t$.

To show this technique, consider the graphical representation in Figure 1b. The nodes are represented by solid diamonds. Time is represented by the vertical axis. The nodal time is represented by black circles and white circles represent the time where linear interpolation was used to obtain the nodal variables at the correct time level.

In the first integration step $\boxed{1}$, the current time is t and the nodes and elements in each group are updated with their corresponding time step. For example, nodes 1 and 2 in group 1 (Δt) are updated to time $t + \Delta t$; the nodes 3 and 4 in group 2 ($2\Delta t$) are updated to time $t + 2\Delta t$ and the nodes 5 and 6 in group 3 ($4\Delta t$) are updated to time $t + 4\Delta t$. Meantime, elements 1 and 2 in group 1 are updated to time $t + \Delta t$, elements 3 and 4 in group 2 are updated to time $t + 2\Delta t$ and the element 5 in group 3 are updated to time $t + 4\Delta t$. It should be noted that nodes 5 and 6 as well as the element 5 needs only one updating to complete the whole cycle because they are integrated with the maximum time step. In the integration step two $\boxed{2}$, the current time is $t+\Delta t$, therefore only nodal and element groups with time step Δt can be updated. Then nodes 1 and 2 as well as elements 1 and 2 in group 1 are updated to time $t+2\Delta t$. To update the element 2 interpolated values of the variables of node 3 at time level $t+\Delta t$ is required. In the third integration sub-cycle $\boxed{3}$, the current time is $t+2\Delta t$, nodes 1 to 4 and elements 1 to 4 are updated. As before, to update elements 2 and 4 in groups 1 and 2 interpolated values of the variables of node 3 and 5 are needed. Finally, time adaption is completed with the fourth and last sub-cycle. In the fourth sub-cycle $\boxed{4}$, only nodes and elements in group 1 are updated.

Updating of different node and element groups is schematically illustrated in Figure 2. In this example, when the current time is $t_c = t$ the group 1 to 3 are updated. In the next time step, the current time is $t_c = t+\Delta t$, hence only the group 1 is updated and so on until the cycle is finished. It should be noted that the current time $t_c = t+4\Delta t$ corresponds to the beginning of a new cycle.

The maximum theoretical gain in processing time (speed-up) using sub-cycles can be calculated by the expression developed by Belytschko and Gilbertsen (1992)

$$speed-up = \frac{t^{nsc}}{t^{sc}} = \frac{NSC}{\sum_{k=1}^{NSC} PESC_k / 100} \tag{16}$$

where t^{nsc} and t^{sc} are the time required to solve a problem with a global time step (without sub-cycles) and using multi-time steps (with sub-cycles), respectively. The number de sub-cycles is NSC and the percentage of elements updated in the sub-cycle k is $PESC$. In this simplified example, fourth sub-cycles are required ($NSC = 4$) and the percentages of elements for groups (g = 1, 2 and 3) are 40%, 40% and 20%, respectively. Therefore, the maximum theoretical gain in processing time is 1.54.

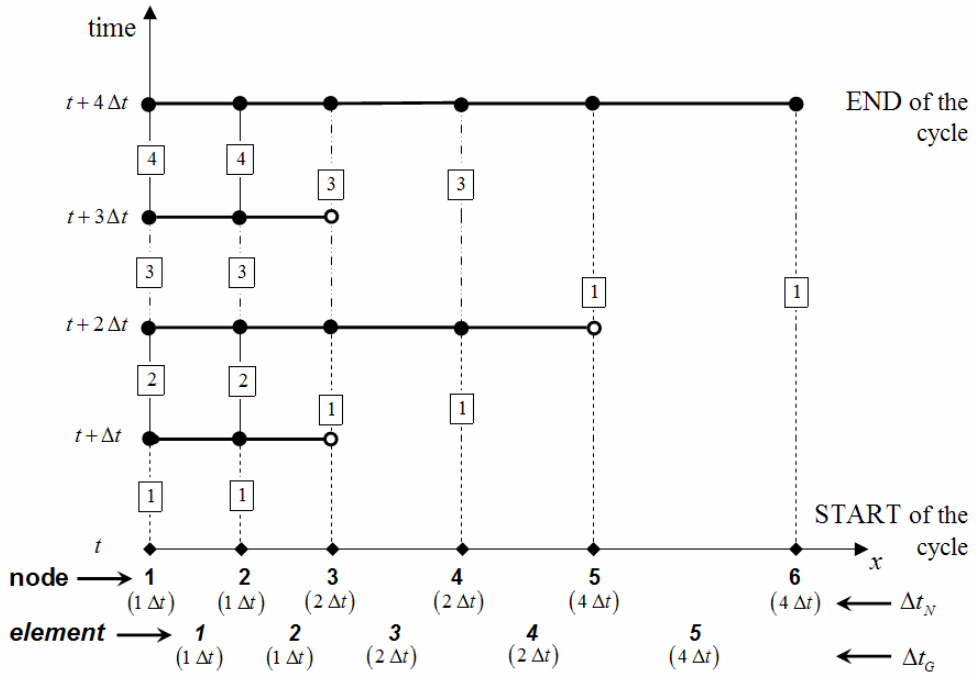

(a)

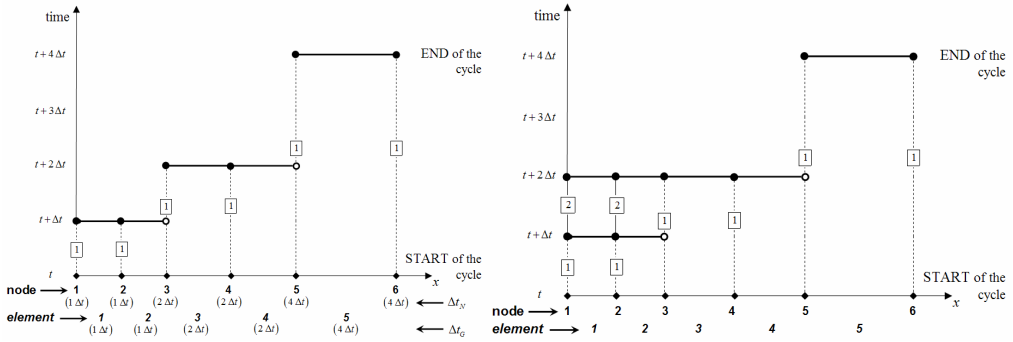

First step Second step

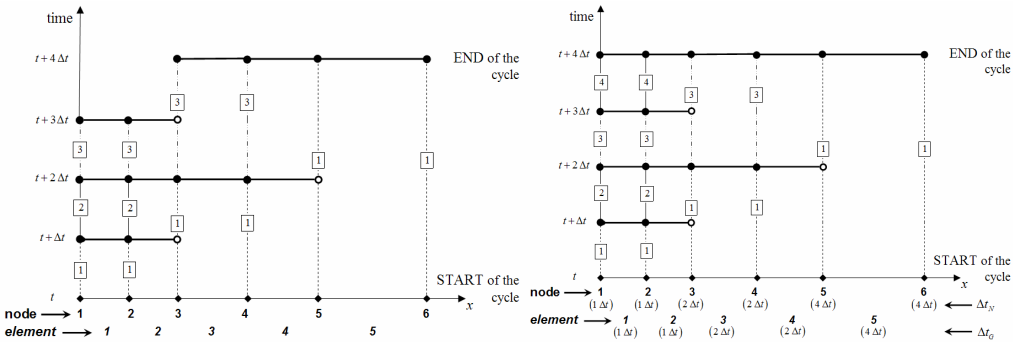

Third step Fourth step

(b)

Figure 1: Graphical representation of the sub-cycle method with three groups of elements. (a) The different steps are presented toghether; (b) Each step is shown separately.

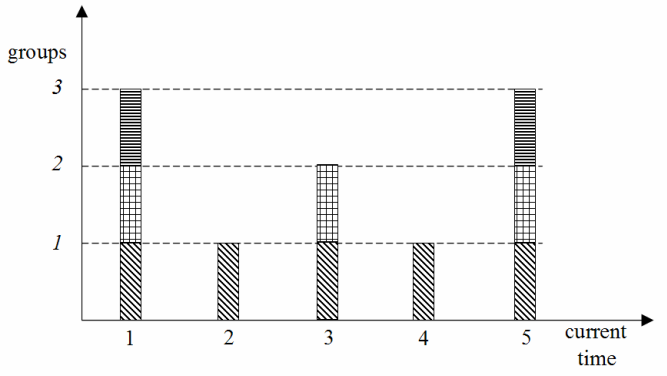

Figure 2: Advancing the node and element groups in the sub-cycle procedure for the one-dimensional problem

6 NUMERICAL RESULTS

In this section, some results for three-dimensional geometries in steady flows are presented. Comparisons are made with experimental data to determine the accuracy, the capability and the performance of the time and space adaptation methodologies.

6.1 Clipped Delta Wing

The evaluation of the efficiency and performance of an adaptive refinement method and a sub-cycle technique is a complicated task due to the numerous aspects that must be considered. In what follows we try to address at least some of them with the help of a classical problem in CFD, such as the clipped delta wing in transonic flow, that we have used in the early stages of development of our code for validation purposes. This wing has been studied experimentally by Bennett and Walker (1999). The wing is characterized by an aspect ratio equal to 1.242, a swept leading edge with 50.4 deg, a unswept trailing edge, and a taper ratio which is take as 0.1423. The airfoil is thus a symmetrical circular arc section with t/c = 0.06.

The two static test cases to study the clipped delta wing (CDW) are given by:

1) Case No. 9E15: inviscid flow at a free stream Mach number equal to 0.901 and an angle of attack equal to 4.24 deg;
2) Case No. 9E11: inviscid flow at a free stream Mach number equal to 1.12 and an angle of attack equal to 0.99 deg.

The simulation for the first and second cases were performed using the same initial mesh (M1=M2) consisting of 76523 linear tetrahedral elements and 15322 nodes. In Table 1 are the identification for each example, the number of nodes (*nno*), the number of elements (*nele*), the number of nodes on the wing (*nnoCS*), the maximum edge length (L_{max}), the minimum edge length (L_{min}) and the minimum time step (Δt).

The adaptive mesh technique is employed in both cases with the following errors indicators: velocity gradients, pressure gradients and specific mass gradients. For more details see Bono (2008). The first and second refinements were identified as R1 and R2, respectively.

To demonstrate improvements due to the adaptive mesh procedure, Figure 3 shows contours of the specific mass on the upper and lower surfaces of the wing corresponding to the initial and final mesh discretizations for the case 9E15 (Mach number = 0.901, angle of attack = 4.24 deg). Note that the upper shock is barely visible in the results obtained with the initial coarse mesh. As expected, considerable improvement in the resolution of the shocks can be observed when an adaptive mesh is employed.

Cases	mesh	*nno*	*nele*	*nnoCS*	L_{max}	L_{min}	Δt
9E15	M1	15322	76523	3979	4.51	1.59×10^{-3}	8.10^{-5}
	M1R1	51269	273689	7782	3.48	7.98×10^{-4}	4.10^{-5}
	M1R2	110725	613017	9701	3.48	3.99×10^{-4}	2.10^{-5}
9E11	M2	15322	76523	3979	4.51	1.59×10^{-3}	8.10^{-5}
	M2R1	35331	188781	4792	3.48	1.59×10^{-3}	5.10^{-5}

Table 1: Numerical parameters for the clipped delta wing simulation.

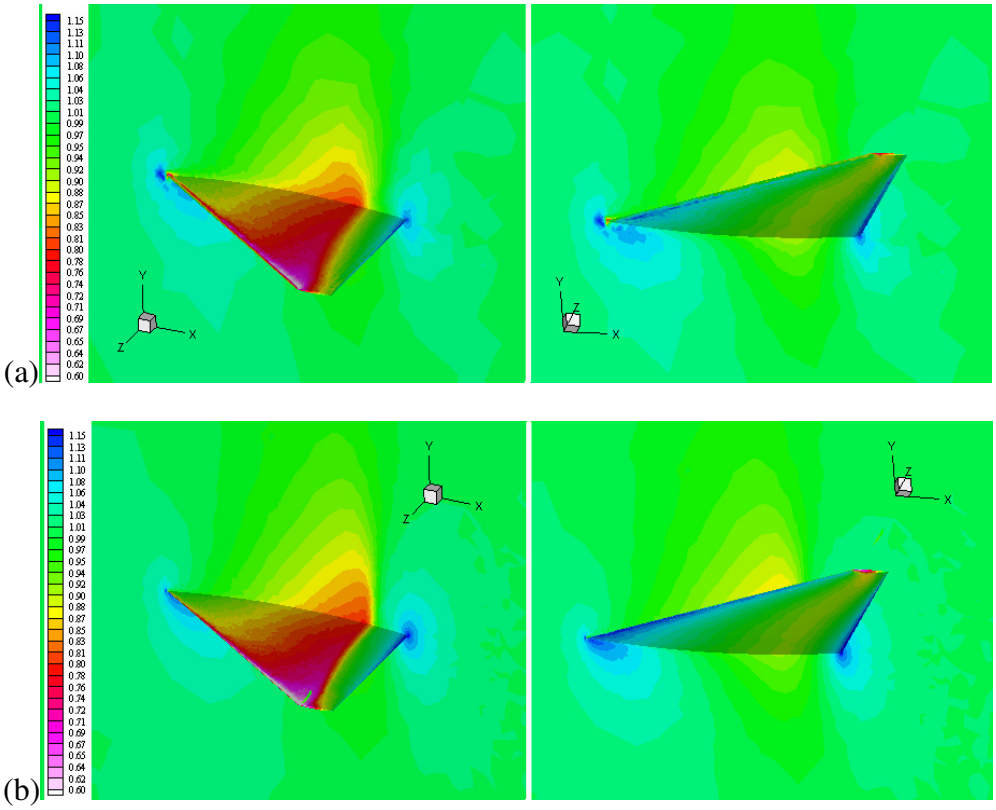

Figure 3: Distribution of the specific mass computed with the initial (a) and final (b) meshes for case 9E15

In Figure 4, the surface pressure distributions obtained with the initial and final mesh are compared with experimental data obtained by Bennett and Walker (1999) for the case 9E15. In general, the surface pressure distributions obtained with the final mesh M1R2 (two refinement levels) compare very well to those obtained from experimental data. From these figures it is clear that initial and final meshes have difficulties to predict the leading edge pressure correctly. Mesh refinement near the leading edge is the unique alternative to obtain better results.

Figure 5 shows the Mach number distributions and the sonic surfaces (M = 1.0) obtained with the initial and final meshes. It can be observed that the sonic surface obtained with the final mesh is larger than that obtained with mesh M1.

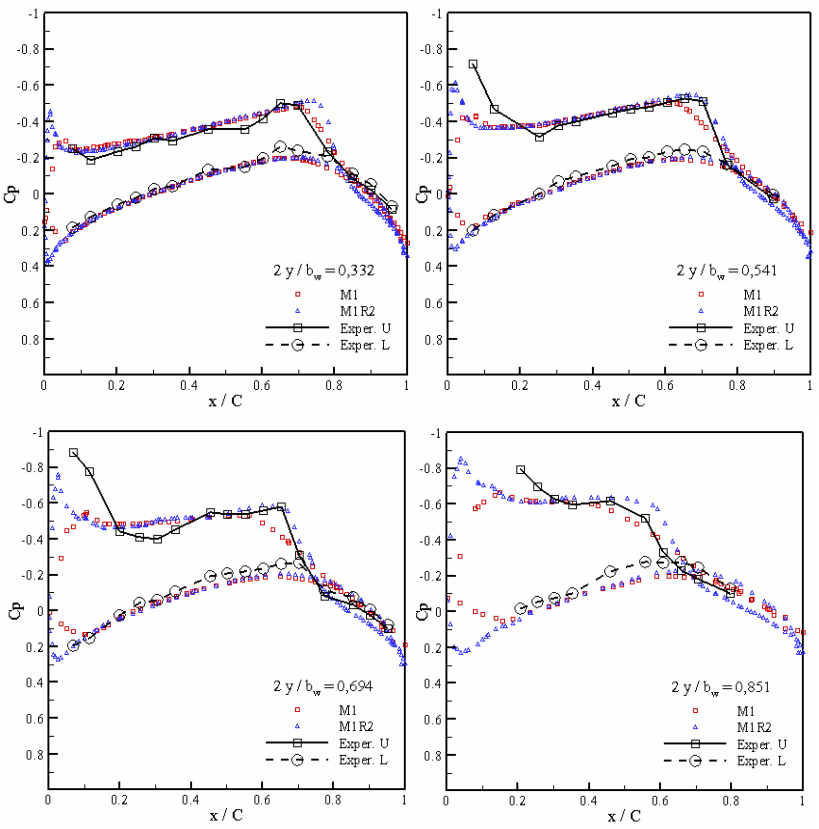

Figure 4: Comparisons of steady pressure distributions using initial and final meshes for case 9E15

(a) 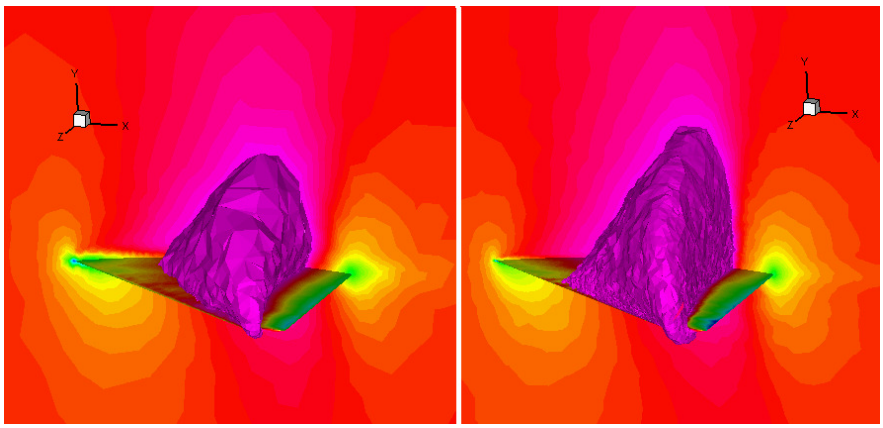 (b)

Figure 5: Mach number distributions and sonic surfaces for the initial (a) and final (b) meshes for case 9E15

Figure 6 shows the specific mass distributions on the upper and lower surfaces of the wing corresponding to the initial and final meshes for the case 9E11 (Mach number = 1.12, angle of attack = 0.99 deg). The leading edge and trailing edge shock waves were efficiently resolved with a mesh refinement.

In Figure 7, the surface pressure distributions obtained with the initial and final meshes are compared with the experimental data obtained by Bennett and Walker (1999) for the case 9E11. The numerical results are in fairly good agreement with the experimental pressure data.

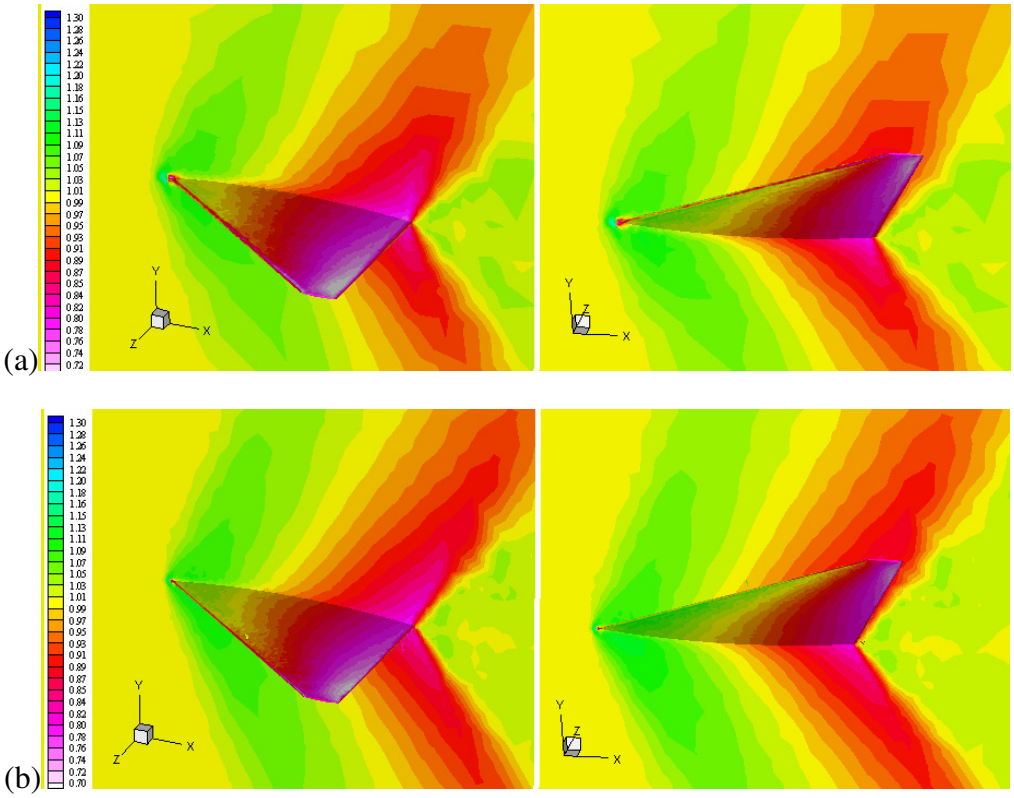

Figure 6: Distribution of the specific mass computed with the initial (a) and final (b) meshes for case 9E11

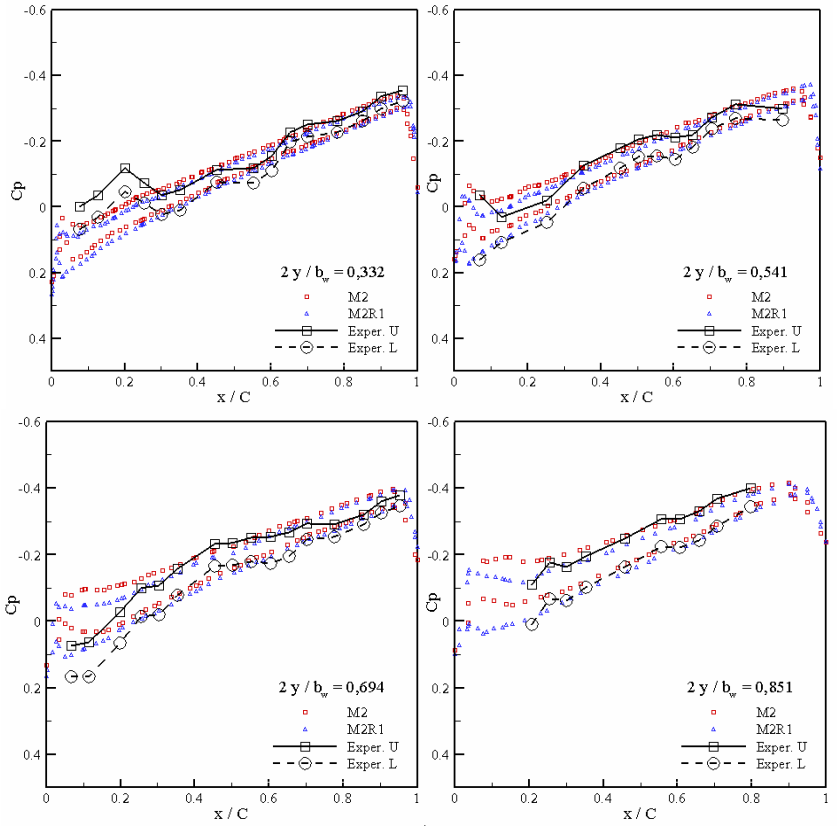

Figure 7: Comparisons of steady pressure distributions using initial and final meshes for case 9E11

To demonstrate the advantages when adaptive spatial and time procedures are combined, Figure 8 shows the pressure coefficient distributions on the upper surface of the clipped delta wing corresponding to the final mesh for the cases 9E15 (mesh M1R2) and 9E11 (M2R1). The results obtained with the time sub-cycles technique was identified as *sc*.

The surface pressure coefficients obtained without the adaptive time procedure compare very well to those obtained including this technique, except for the small discrepancies that are evident near the leading edge in both cases and the trailing edge region in the case 9E11. These oscillations only occur in regions of the mesh where there is an abrupt transition from fine to coarse elements.

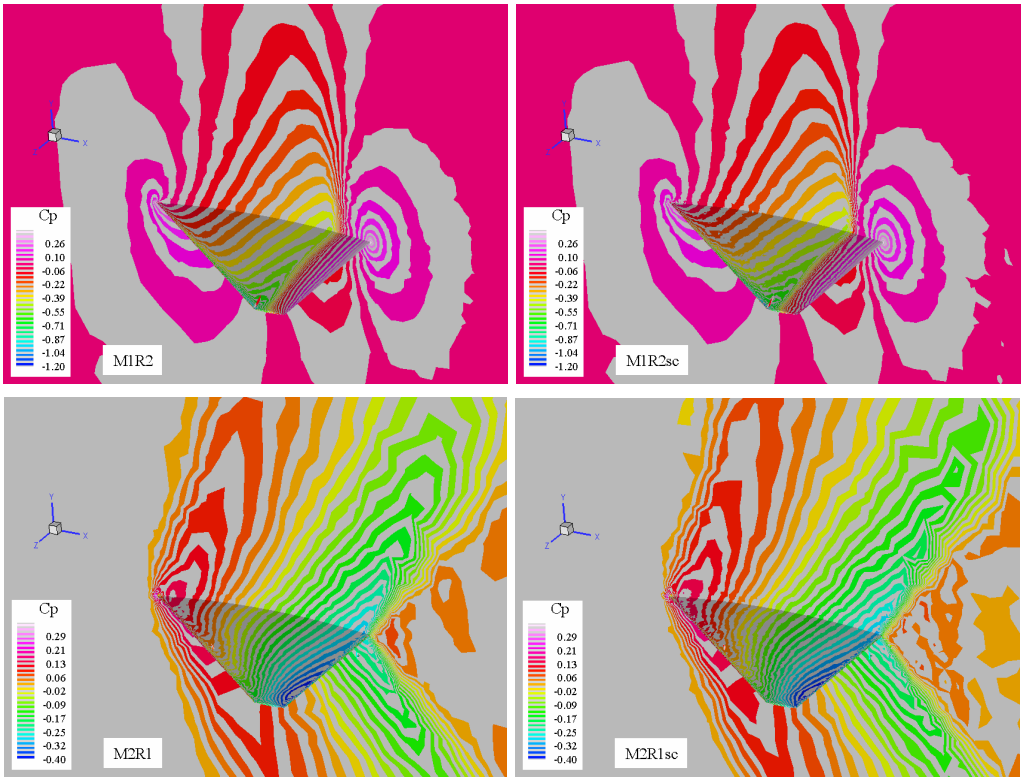

Figure 8: Pressure coefficient distribution on the meshes M1R2 and M2R1 for test cases 9E15 and 9E11

In Table 2, the percentage of elements belonging to each element group, the maximum theoretical speed-up ($\boldsymbol{S\text{-}U_{theo}}$) and maximum real speed-up ($\boldsymbol{S\text{-}U}$) are presented for the clipped delta wing problem. These results show that the sub-cycles technique in meshes M1R1 and M1R2 are approximately 1.68 and 2.39 times faster than cases where a unique global time step was adopted. For mesh M2R1 the value of the theoretical computational saving is 1.30. The two main reasons for differences between theoretical and real speed-up have been identified. The first reason is that the operations to control groups of nodes and elements increase the processing time. The second reason is that the performance decreases because there are loops executed only for groups which must be updated at a given instant, introducing indirect addressing.

The time steps distributions over the clipped delta wing on the final meshes for the cases 9E15 and 9E11 are shown in Figure 9. It should be noted that the minimum time step ($1\Delta t$ and $2\Delta t$) are localized in the leading and trailing edges. The medium time step ($4\Delta t$ to $16\Delta t$) are located around the wing and the maximum time step ($32\Delta t$ to $128\Delta t$) are located relatively far from the wing.

Group	M1R1	M1R2	M2R1
1 Δt	0.318	0.146	5.098
2 Δt	11.659	2.585	36.343
4 Δt	48.948	23.426	25.367
8 Δt	17.919	30.401	18.133
16 Δt	10.031	17.344	5.418
32 Δt	3.866	11.590	1.442
64 Δt	1.027	4.224	2.591
128 Δt	6.231	10.283	5.607
***S-U*$_{theo}$**	***4.66***	***7.88***	***3.09***
S-U	**1.68**	**2.39**	**1.30**

Table 2: Percentage of elements belonging to each element group.

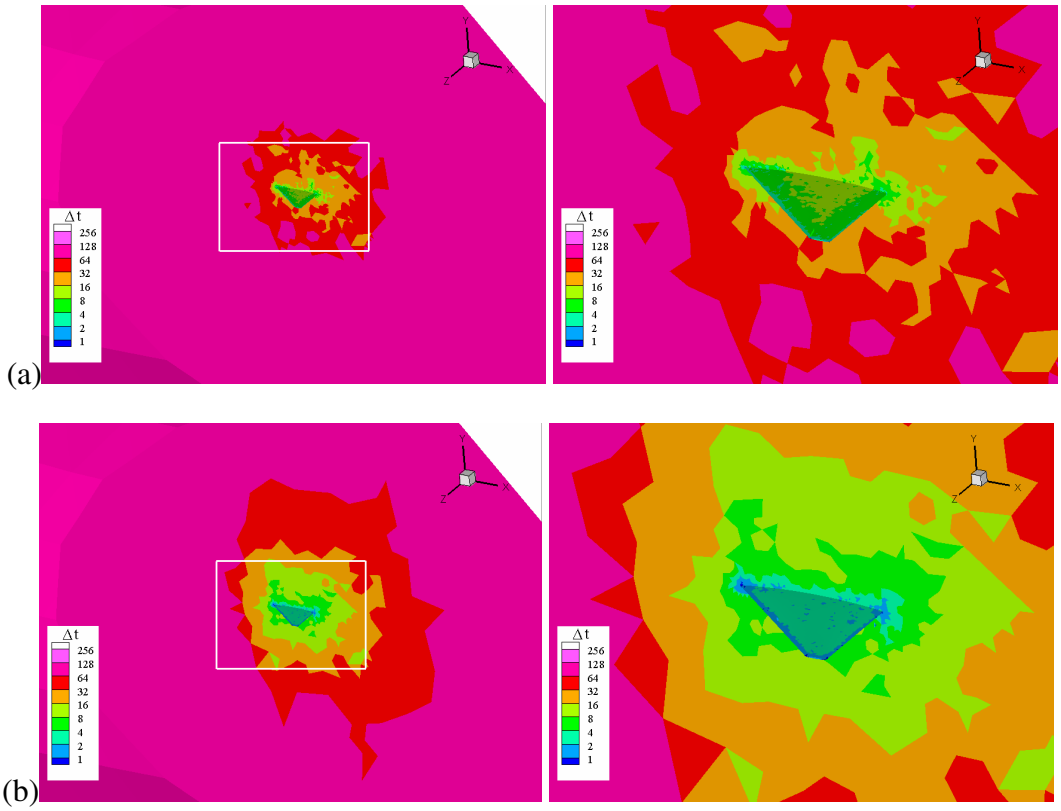

Figure 9: Time steps distributions on the meshes M1R2 (a) and M2R1 (b) for test cases 9E15 and 9E11

Finally, in Figure 10 the pressure coefficient distributions obtained with the time adaptive technique are compared with the distributions obtained without sub-cycles. Both cases agree well. However, in the tip of the wing, small discrepancies are evident when results obtained with sub-cycles are compared with those obtained without sub-cycles.

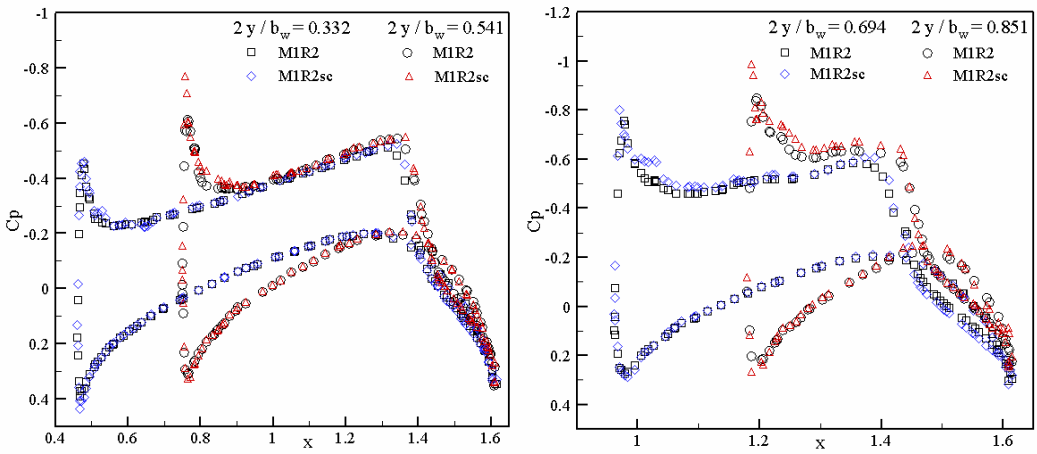

Figure 10: Pressure coefficient distribution on the meshes M1R2 with and without sub-cycles for test cases 9E15

7 CONCLUSIONS

The aim of this work is to provide an study of an algorithm which combines an automatic adaptive strategy and explicit multi-time steps integration technique in the solution of unstructured finite element problems. The time-spatial adaptation method is tested here with the steady three-dimensional Euler equations in transonic flow over a clipped delta wing.

Results in the previous section show that a time adaptive method, when combined with a mesh adaptive technique can be used for practical applications and that it is substantially faster than comparable methods without sub-cycles. Based on the results obtained here, it may be concluded that an automatic adaptive technique have produced important improvements. Multi-time steps using sub-cycles is a fast and efficient procedure and it is easy to implement. The algorithm is stable and its efficiency is expressed in terms of the speed-up which varies from 1.3 to 2.39 with respect to simulations with time step uniform.

The time-spatial adaptive methods implemented herein was shown to produce solutions comparable in accuracy to others without sub-cycles, but the computational efficiency was lower than expected. The main reason for the relative computational “inefficiency” has been identified; the elements in the regions of high gradients of some flow characteristic must be refined in order to obtain adequated spatial resolution of the flow features. This leads to a large number of small elements and results in an increase of the total number of elements having the minimum time step ($1\Delta t$ to $4\Delta t$), which inhibits the performance of the time adaptive procedure since it reverts to the use of a unique global time step. More work needs to be done to improve the speed-up studying further code optimization, and future parallelization of the code. Summarizing, the main contribution of the work is the formulation of a time-spatial adaptive procedure, which is integrated with an explicit one-step Taylor-Galerkin scheme to simulate inviscid compressible flows.

Acknowledgements

The first author gratefully acknowledges the support of the CAPES (Doctoral scholarship).

REFERENCES

Argyris, J., Doltsinis, I.S., and Friz, H. Study on computational reentry aerodynamics. *Computer Methods in Applied Mechanics and Engineering*, 81:257–289, 1990.

Belytschko, T., and Gilbertsen, N.D. Implementation of Mixed Time Integration Techniques on a Vectorized Computer with Shared Memory. *Int. J. Num. Meth. Eng.*, 35: 1803-1828, 1992.

Belytschko, T., and Lu, Y.Y. Explicit Multi-time step integration for first and second order finite element semidiscretizations. *Comput. Methods Appl. Mech. and Engrg.*, 108: 353-383, 1993.

Belytschko, T., Yen, H.J., and Mullen, R. Mixed Method for Time Integration. *Comput. Methods Appl. Mech. and Engrg.*, 17/18: 259-275, 1979.

Bennett, R.M., and Walker, C.E. Computational Test Cases for a Clipped Delta Wing With Pitching and Trailing-Edge Control Surface Oscillations, *TM-209104, NASA*, 1999.

Bono, G. *Simulação Numérica de Escoamentos em Diferentes Regimes utilizando o Método dos Elementos Finitos (text in portuguese)*. Doctoral Thesis, PROMEC, UFRGS, Brazil, 2008.

Bono, G., Popiolek, T.L., and Awruch, A.M. Estrategia de Adaptación de Mallas para Problemas Aeroespaciales y Aeronáuticos (text in spanish), *Mecánica Computacional (Proceedings of the ENIEF 2007, Córdoba, Argentina)*, 26, 3117-3133, 2007.

Chang, H.J., Bass, J.M., Tworzydlo, W., and Oden, J.T. H-P Adaptive Methods for Finite Element Analysis of Aerothermal Loads in High-speed Flows. *CR-189739, NASA*, 1993.

Donea, J.. A Taylor-Galerkin for convective transport problems. *International Journal for Numerical Methods in Engineering*, 20:101–119, 1984.

Hooker, J.R., Batina, J.T., and Williams, M.H. Spatial and temporal adaptive procedures for the unsteady aerodynamic analysis of airfoils using unstructured meshes. *Technical Memorandum TM-107635*, NASA, 1992.

Hughes, T.J.R., and Liu, W.K. Implicit-explicit Finite Element in Transient Analysis: Stability Theory. *Journal Appl. Mech.*, 45: 371-374, 1978.

Hughes, T.J.R., and Tezduyar, T.E. Finite element methods for first-order hyperbolic systems with particular emphasis on the compressible Euler equations. *Computer Methods in Applied Mechanics and Engineering*, 45:217–284, 1984.

Löhner, R. *Applied CFD Techniques. An Introduction based on Finite Element Methods*. John Wiley & Sons Ltd., England, 2001.

Löhner, R., Morgan, K., and Zienkiewicz, O.C. The Solution of Non-linear Hyperbolic Equation Systems by the Finite Element Method. *International Journal for Numerical Methods in Fluids*, 4: 1043-1063, 1984.

Maurits, N.M., van der Ven, H., and Veldman, A.E.P. Explicit multi-time stepping for convection-dominated flow problems. *Comp. Meth. Appl. Mech. and Eng.*, 157: 133-150, 1998.

Popiolek, T.L., and Awruch, A.M. Numerical Simulation of Incompressible Flows using Adaptive Unstructured Meshes and the Pseudo-compressibility Hypothesis. *Advances in Eng. Soft.*, 37: 260-274, 2006.

Teixeira, P.R.F., and Awruch, A.M. Three-dimensional Simulation of High Compressible Flows using a Multi-time-step Integration Technique with Subcycles. *Appl. Math. Modelling*, 25: 613-627, 2001.

van der Ven, H., Niemann-Tuitman, B.E., and Veldman, A.E.P. An explicit multi-time-stepping algorithm for aerodynamic flows. *Journal Comp. Appl. Mathematics*, 82: 423-431, 1997.

Wackers, J., and Koren, B. A simple and efficient space-time adaptive grid technique for unsteady compressible flows. *Proceedings 16th AIAA Computational Fluid Dynamics Conference*, AIAA-paper 2003-3825, USA, 2003.